J. Fluid Mech. (2014), *vol.* 747, *pp.* 30–43.
doi:10.1017/jfm.2014.140

A minimal flow-elements model for the generation of packets of hairpin vortices in shear flows

Jacob Cohen†, Michael Karp and Vyomesh Mehta

Faculty of Aerospace Engineering, Technion – Israel Institute of Technology, Haifa 32000, Israel

(Received 5 November 2013; revised 3 February 2014; accepted 9 March 2014;
first published online 10 April 2014)

Packets of hairpin-shaped vortices and streamwise counter-rotating vortex pairs (CVPs) appear to be key structures during the late stages of the transition process as well as in low-Reynolds-number turbulence in wall-bounded flows. In this work we propose a robust model consisting of minimal flow elements that can produce packets of hairpins. Its three components are: simple shear, a CVP having finite streamwise vorticity magnitude and a two-dimensional (2D) wavy (in the streamwise direction) spanwise vortex sheet. This combination is inherently unstable: the CVP modifies the base flow due to the induced velocity forming an inflection point in the base-flow velocity profile. Consequently, the 2D wavy vortex sheet is amplified, causing undulation of the CVP. The undulation is further enhanced as the wave continues to be amplified and eventually the CVP breaks down into several segments. The induced velocity generates highly localized patches of spanwise vorticity above the regions connecting two consecutive streamwise elements of the CVP. These patches widen with time and join with the streamwise vortical elements situated beneath them forming a packet of hairpins. The results of the unbounded (having no walls) model are compared with pipe and channel flow experiments and with a direct numerical simulation of a transition process in Couette flow. The good agreement in all cases demonstrates the universality and robustness of the model.

Key words: instability, transition to turbulence, vortex dynamics

1. Introduction

At sufficiently low speeds the motion of fluids is laminar but becomes highly disordered and turbulent when the velocity is increased beyond a certain threshold. Whereas in a laminar flow two adjacent 'fluid particles' move nearly parallel to each other and do not cross the trajectories of each other, turbulent flows are characterized by trajectories crossing. If the crossing of the trajectories is localized in space and random in time, the flow seems chaotic, three-dimensional and has a wide and continuous spectrum of scales. Theodorsen (1952) proposed a basic vortex structure having the shape of a horseshoe (or hairpin) inclined at 45° to the main flow and therefore can act as a pump transporting momentum in the cross-flow direction (according to the Biot–Savart law). It is composed of a pair of inclined streamwise

† Email address for correspondence: aerycyc@gmail.com

(downstream) vortices connected by a short spanwise 'head' segment. Its associated velocity field consists of an upstream and outward induced velocity between the hairpin 'legs' and vortex flow around its 'head', resulting in significant mixing which is a major characteristic of turbulent shear flows.

In recent years it has become evident that the building blocks of low-Reynolds-number wall-bounded turbulent shear layers are very similar to those observed during the late stages of the transition process. In particular, packets of hairpin-shaped vortices and streamwise counter-rotating vortex pairs (CVPs) seem to dominate both kinds of flow. Striking similarities between the characteristics of CVPs, such as their spanwise wavelength and streamwise extent, in transitional and turbulent flat-plate boundary layers have been observed by Blackwelder (1983) and Swearingen & Blackwelder (1987). Similarly, Skote, Haritonidis & Henningson (2002) have observed similarities between the horseshoe vortices in turbulent and laminar boundary layers. Therefore, studying the evolutionary dynamics of artificially generated vortical disturbances in various subcritical wall-bounded shear flows provides insight on their evolution in the turbulent field. Experimental examples of such studies concerning CVPs breakdown and consequent formation of packets of hairpins have been documented in a laminar boundary layer by Acarlar & Smith (1987) using a hemisphere protuberance and by Haidari & Smith (1994) using pulsed injection from a streamwise slot; in a rotating axisymmetric Couette flow (Levinski & Cohen 1995; Malkiel, Levinski & Cohen 1999); in a subcritical channel flow (Philip, Svizher & Cohen 2007); and in a pipe Poiseuille flow (Peixinho & Mullin 2007). Furthermore, in the latter paper, the packet of hairpins is observed to be an integral part of the transition process (cf. figure 5 therein).

Recently, using a direct numerical simulation (DNS), a forest of hairpins was found to dominate the late transition stages of a laminar boundary layer over a flat plate (Wu & Moin 2009) and in particular local regions of turbulent spots (Strand & Goldstein 2011). Although a number of investigators have deduced from their own measurements or postulated the existence of such structures in turbulent shear flows (e.g. Robinson 1991; Adrian, Meinhart & Tomkins 2000; Hutchins, Hambleton & Marusic 2005), such direct evidence for their dominance has not been reported in the past since the flow visualization experiments in turbulent boundary layers by Head & Bandyopadhyay (1981). More recently, similar forests of hairpins have been observed by other investigators, e.g. Chu & Goldstein (2012) and Rist (2012).

A recent series of studies by Cherubini *et al.* (2010*a*,*b*, 2011*b*) has concentrated on finding the minimal seed, i.e. the smallest structure by which the maximum energy growth is achieved over short times, triggering transition in a boundary layer. Using an optimization process combined with DNS, it was found that the optimal initial perturbation is characterized by a pair of streamwise-modulated counter-rotating vortices, tilted upstream. The resulting transition process was characterized by the appearance of hairpin vortices and streamwise streaks. Moreover, these structures have been found as localized flow structures living on the edge of chaos (Cherubini *et al.* 2011*a*; Duguet *et al.* 2012).

A mechanism for the generation of a packet of hairpins in a fully developed turbulent channel flow was proposed by Zhou, Adrian & Balachandar (1996), Zhou *et al.* (1999) using DNS, where the key element is a single strong hairpin vortex. When the magnitude of the initial vortex exceeds a certain threshold relative to the mean flow, new offspring hairpin vortices are generated upstream and downstream of the primary vortex, forming a coherent packet of hairpins. A similar offspring auto-generation process was observed experimentally by Adrian *et al.* (2000) in a

turbulent boundary layer. In these cases, the resulting packet consists of several hairpins with different strength, the envelope shape of which resembles a wedge. Such packets in turbulence are also in part supported by the attached eddy model calculation (Marusic 2001).

A different mechanism for the generation of a train of hairpin vortices in turbulent boundary layers is related to a normal inflectional instability of the streaks (Skote *et al.* 2002), associated with a varicose mode. In this DNS study laminar and turbulent boundary layers have been subjected to continuous blowing through a streamwise slot. The occurrence of hairpin vortices under varicose streak instability was also found experimentally in a laminar boundary layer by Asai, Minagawa & Nishioka (2002).

In summary, two main mechanisms for the formation of packets of hairpins have been proposed. Both models have been demonstrated via DNS or experiments in turbulent (and laminar) wall-bounded shear flows. The offspring mechanism relies on a certain hierarchy of the hairpins within the packet, whereas the instability-based mechanism suggests that a varicose secondary perturbation of a streak leads to a train of hairpins. The offspring mechanism is not supported by a certain mathematical model and explains the physics of the generation process qualitatively. The instability-based mechanism demonstrates that for turbulent (and laminar) boundary layers subjected to jet injection (or a bump) the origin of the train of hairpins is due to inflectional instability. However, it is hard to isolate the key elements governing the process as it contains the entire complex flow field.

The purpose of the current study is to propose a simple (synthetic) universal model, related to the instability-based mechanism, for the formation of a packet of hairpin vortices. In particular, the model highlights the minimal key elements required for the generation of such a packet and explains the associated physical process. The minimal number of key elements assures the robustness of the model as it does not include walls (or any other boundary conditions) as well as a particular base-flow velocity profile (besides simple shear). As such, the model is universal and can be tested in different geometries such as pipe, channel and boundary-layer flows. The model results are compared with experiments in pipe and channel flows as well as DNS of transitional Couette flow.

2. The model for generating a packet of hairpins

Following ideas first presented at the Global Flow Instability and Control IV symposia (Cohen, Karp & Shukhman 2009), we propose the present model which is independent of a specific geometry or flow conditions. The model does not seek for the minimal disturbance energy required for transition; instead it offers the minimal (three) basic flow elements (introduced synthetically) required for the formation of a packet of hairpins. Here we concentrate on parallel base flows having a velocity field $\boldsymbol{V} = (U(y), 0, 0)$, which is also a good approximation for high-Reynolds-number boundary layers. The coordinate system has the x-, y- and z-axes aligned in the streamwise, cross-stream and spanwise directions, respectively.

A key element of the proposed model is the interaction between a localized vortical disturbance and its surrounding base flow. Such an interaction has been described by Suponitsky, Cohen & Bar-Yoseph (2005) and serves as a building block of the current model. Owing to its localization the surrounding velocity field can be approximated by Taylor series. Thus, in a coordinate system attached to its centre, the vortical disturbance mainly 'sees' a simple shear as illustrated in figure 1(a) (i.e. the cross-stream gradient $\mathrm{d}U/\mathrm{d}y = -\Omega$, is assumed constant, where Ω is the spanwise vorticity, $\boldsymbol{\Omega} = curl(\boldsymbol{V}) = (0, 0, \Omega)$).

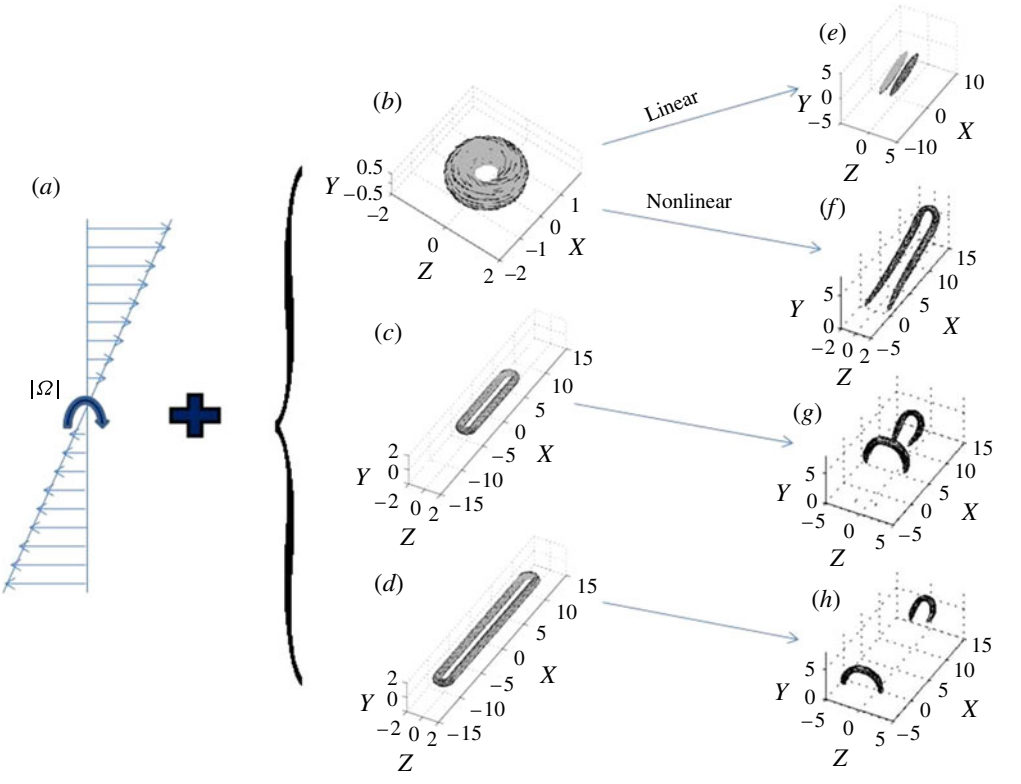

FIGURE 1. The interaction between pure shear (*a*) and a localized disturbance having a single length scale (*b*) and two length scales (*c*,*d*). When the magnitude of the localized vortex (*b*) is small a CVP is evolved (*e*) whereas when it is finite a hairpin is formed (*f*). When the magnitude of the elongated vortex (*c*,*d*) is high and the aspect ratio between the streamwise and spanwise length scales exceeds a certain threshold, two hairpins are formed at both streamwise ends (*g*,*h*). The aspect ratio is 5 and 10 for (*c*) and (*d*), respectively. (Figure reproduced from Suponitsky *et al.* (2005).)

In the following we first summarize briefly previous results describing the interaction between a localized vortical disturbance and its surrounding base flow (Suponitsky *et al.* 2005). Then, we devise the present model for the generation of a packet of hairpins, based on the observed mechanisms associated with the localized disturbance.

The interaction between simple shear (figure 1*a*) and a localized vortex having a single length scale (figure 1*b*) can lead to the formation of a single CVP if the initial magnitude is relatively small (figure 1*e*) or a hairpin vortex (figure 1*f*) if it is sufficiently high (Suponitsky *et al.* 2005). In figure 1(*c*,*d*) the case of an initial elongated vortex having two length scales in the streamwise and spanwise directions is introduced. For sufficiently strong initial vortices and beyond a certain threshold of the aspect ratio between the streamwise and spanwise lengths of the vortex ($\approx$5), the interaction with the shear of the base flow leads to the evolution of two hairpins at both ends of the elongated structure (figure 1*g*,*h*, Suponitsky *et al.* 2005). As the aspect ratio is further increased, the length of the central CVP segment is also increased and similar results are obtained (not shown here).

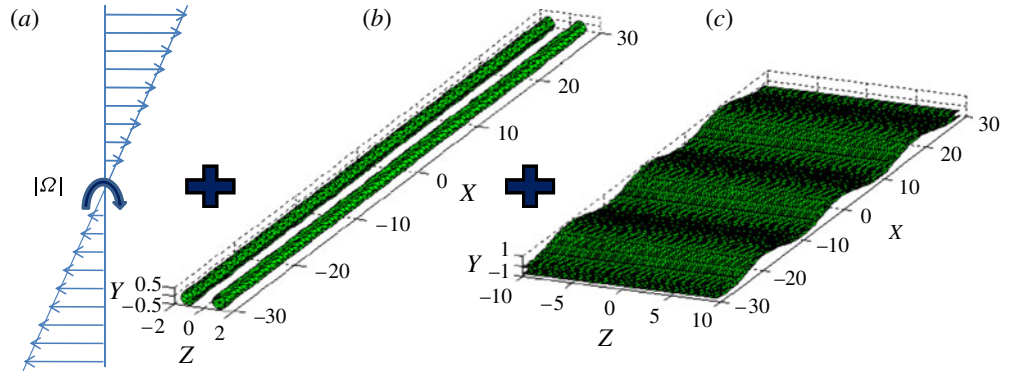

FIGURE 2. (Colour online) Illustration of the three elements of the model: (*a*) simple shear; (*b*) CVP; (*c*) 2D wavy vortex sheet.

The above results indicate that the formation of hairpins occurs where the streamwise vorticity of the CVP segment has sharp gradients in the streamwise direction. Therefore, a localized vortical disturbance cannot produce more than two hairpin vortices. Consequently, in order to generate a packet consisting of three or more hairpins, streamwise variation of the CVP is required.

The above findings imply that a long CVP undergoing streamwise variation will evolve into a packet of hairpins. This suggests a three-elements model consisting of a straight CVP having finite streamwise vorticity magnitude, embedded in simple shear and subjected to a 2D wavy (in the streamwise direction) disturbance (a vortex sheet having only spanwise vorticity). The three elements are schematically illustrated in figure 2. This combination is inherently unstable: the CVP modifies the base flow due to the induced velocity (via the Biot–Savart law), causing an inflection point in the base-flow velocity profile. This leads to the well-known inviscid instability mechanism (Rayleigh 1880). Consequently, the two-dimensional (2D) wave is amplified, causing undulation of the CVP. The undulation is further enhanced as the wave continues to be amplified. Eventually, the strong variation in the streamwise vorticity of the CVP results in its breakdown into several segments and leads to the formation of a packet of hairpins (as detailed below).

To demonstrate the generation of a packet of hairpins in accordance with the above model, we employ a recently developed analytical-based numerical method (Cohen *et al.* 2010). It is capable of following the evolution of finite-amplitude localized vortical disturbances embedded in unbounded viscous shear flows. In other words, the method is a fully nonlinear, three-dimensional and viscous DNS code, specifically designed to follow the evolution of localized disturbances embedded in base flows having constant shear. The solution is carried out using Lagrangian variables in Fourier space which enables efficient and much faster computations than other DNS software. The method, implemented in Matlab, was successfully validated by comparing its results with those obtained by the commercial software Fluent (Suponitsky *et al.* 2005, presented in figure 1) and with additional results (Cohen *et al.* 2010).

The use of Fourier space in the model allows us also to follow the evolution of periodic (in space) disturbances. In particular, the method enables us to follow the evolution of the disturbance associated with the three-element model proposed above. Thus, the method is used to follow the evolution of a CVP and a wavy 2D vortex

sheet embedded in simple shear. Accordingly, the initial disturbance (at time $t=0$) is composed of a synthetic CVP having streamwise vorticity (ω_x) and a wavy spanwise vortex-sheet disturbance (ω_z). Their respective mathematical expressions are

$$\omega_x = \varepsilon\Omega \exp\left(-\frac{y^2}{\delta^2}\right)\left\{-\exp\left(-\frac{(z-d_0)^2}{\delta^2}\right)+\exp\left(-\frac{(z+d_0)^2}{\delta^2}\right)\right\}, \tag{2.1}$$

$$\omega_z = a_0\Omega \exp\left\{-\frac{(y-h_0\cos(2\pi x/\lambda))^2}{\delta^2}\right\}, \tag{2.2}$$

where $\varepsilon = \max\{\omega_x(t=0)\}/|\Omega|$ is the normalized vorticity magnitude of the CVP, $2d_0$ is the separation distance between the vortices and δ represents the thickness of each vortex. In the expression for the spanwise vortex sheet (2.2), a_0 is its magnitude (normalized by $|\Omega|$), h_0 is the height of the modulation and λ is its streamwise wavelength. All variables are made non-dimensional using $|\Omega|$ and δ. In the following, the non-dimensional coordinates and time are indicated by capital letters (X, Y, Z and T, respectively).

An example demonstrating the temporal evolution of the initial disturbance is presented in figure 3. To identify the vortical structure, Q, the second invariant of the velocity gradient tensor, is used ($Q = -0.5\partial u_i/\partial x_j \cdot \partial u_j/\partial x_i$; see Hunt, Wray & Moin 1988). The parameters used here are: $\Omega = -40$ (s^{-1}), $\nu = 10^{-6}$ ($\mathrm{m}^2\ \mathrm{s}^{-1}$), $\delta = 1$ mm, $\varepsilon = 7.5$, $d_0 = \delta$, $\lambda = 10\delta$, $a_0 = 0.5$ and $h_0 = 0.5\delta$. The CVP is initially straight (figure 3*a*). The inflection point formed by the CVP induced velocity causes an inviscid instability, leading to its undulation. At $T = 2$ (figure 3*b*) the waviness is further enhanced and the CVP is about to be separated into six periodical patches of vortex elements. Consequently, at $T = 2.5$ (figure 3*c*) a spanwise vortex segment is formed above the regions connecting two consecutive streamwise elements of the CVP, where a relatively strong variation of the induced velocity along the streamwise direction exists ($\partial v/\partial X$). With time the top spanwise vortical segments widen and join with the streamwise vortical elements situated beneath them forming a packet of hairpins (see $T = 3.5$, 4 in figure 3*d*,*e*, respectively).

The induced velocity and its streamwise derivative are shown in figure 4 for time $T = 2.5$. The relatively strong streamwise variation of the induced velocity at the wall-normal location of the spanwise vortical segments ($Y = 3.4$, $Z = 0$) can be seen in figure 4(*a*). The maximal spanwise vorticity (associated with the negative peaks of $\partial v/\partial X$) is periodically positioned at the streamwise locations of $X = -16.9$, -7.0, 2.8 and 13.1 (figure 4*b*), corresponding to the streamwise locations of the spanwise vortical segments shown in figure 3(*f*) for $T = 2.5$. The wall-normal distribution of $\partial v/\partial X$ at $X = 2.8$ is shown in figure 4(*c*). As can be seen, the maximal spanwise vorticity is indeed at $Y = 3.4$, where the spanwise vortical segments are located. (It should be noted that $Y = 0$ corresponds to the initial location of the vortices.)

The above-described scenario may explain observations of packets of hairpins in transitional wall-bounded shear flows (and perhaps low-Reynolds-number turbulent boundary layers as well). In fact, if we follow the inclination angle of the evolved packet, i.e. the side views of the 'bridges' connecting the top spanwise vortical 'heads' with the bottom streamwise 'legs', it can be seen that by $T = 5$ (figure 3*f*) the inclination angle is $\sim 45^\circ$, which agrees with previous observations of hairpins in turbulent boundary layers (e.g. Head & Bandyopadhyay 1981).

A key element in the above mechanism is the existence of inflection points in the velocity profile. In this regard, a simple control mechanism was demonstrated by Hof *et al.* (2010), where turbulence in intermittent pipe flow was eliminated by

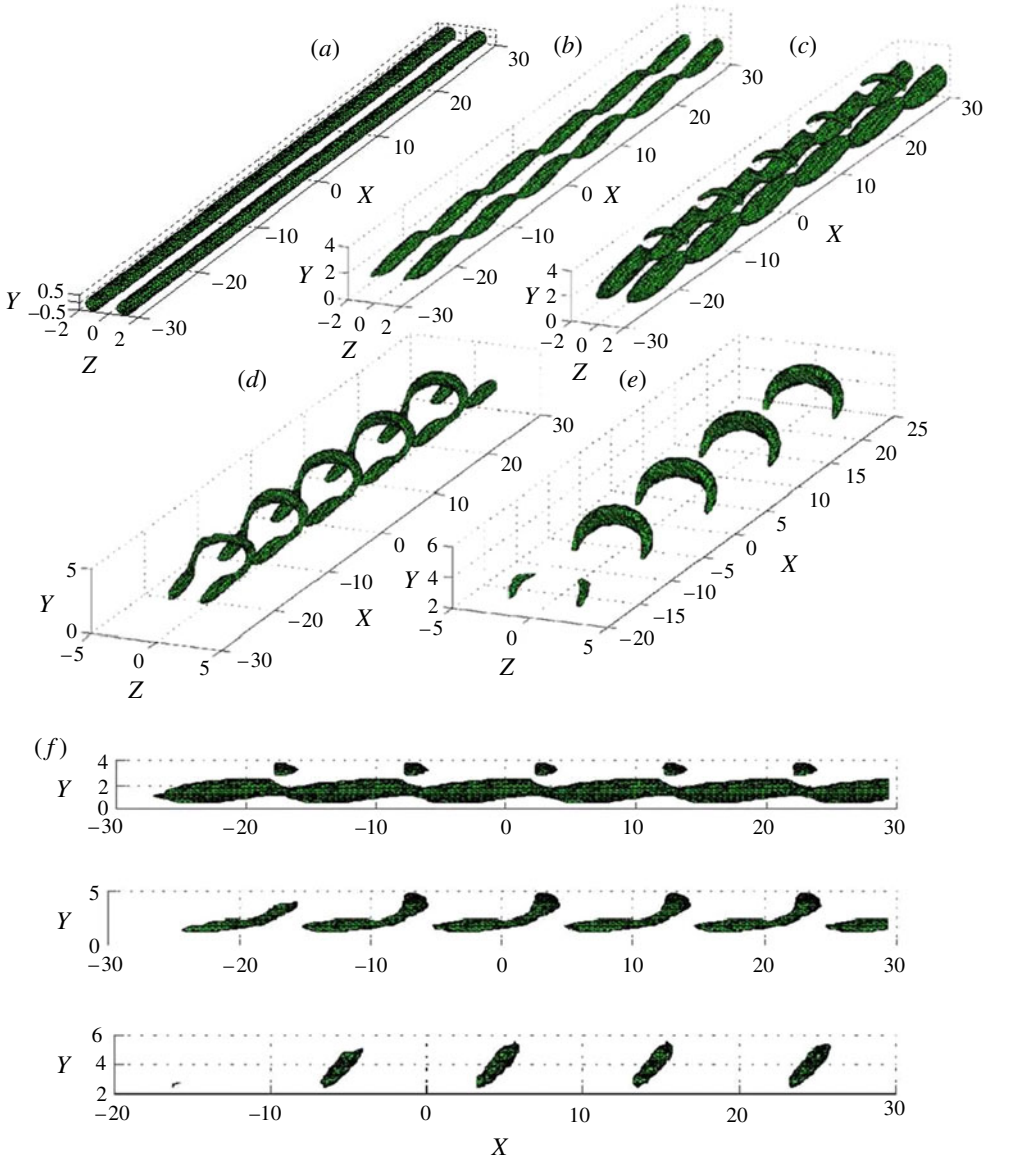

FIGURE 3. (Colour online) The temporal evolution of a packet of hairpins from a wavy spanwise vortex sheet imposed on a CVP embedded in simple shear: (*a*) $T = 0$, $Q/Q_{max} = 0.6$; (*b*) $T = 2$, $Q/Q_{max} = 0.6$; (*c*) $T = 2.5$, $Q/Q_{max} = 0.3$; (*d*) $T = 3.5$, $Q/Q_{max} = 0.3$; (*e*) $T = 4$, $Q/Q_{max} = 0.3$; (*f*) side views, $Q/Q_{max} = 0.1$ from top to bottom $T = 2.5$, $T = 3.5$ and $T = 5$. The parameters are: $\Omega = -40$ (s^{-1}), $\nu = 10^{-6}$ ($m^2\ s^{-1}$), $\delta = 1$ mm, $\varepsilon = 7.5$, $d_0 = \delta$, $\lambda = 10\delta$, $a_0 = 0.5$ and $h_0 = 0.5\delta$. The structures are shown by isosurfaces of the Q definition.

reducing inflection points in the velocity profile. Another key element of the model is the coexistence of large-scale structures (e.g. the elongated CVP) and localized disturbances. This resembles the separation of scales by Marusic, Mathis & Hutchins (2010) which enabled them to formulate a predictive model for turbulent flows.

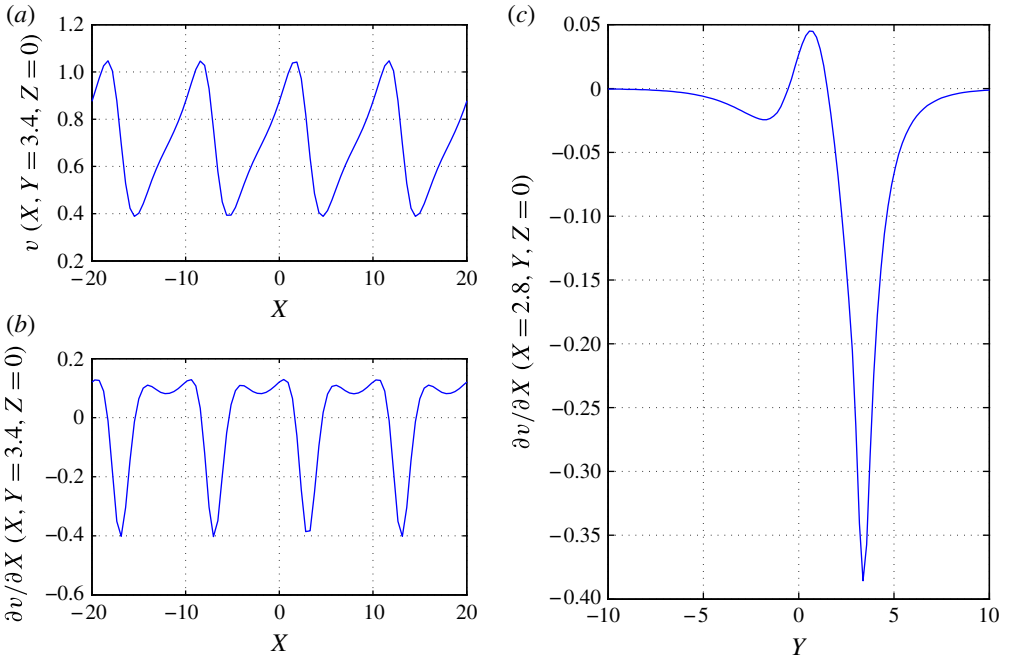

FIGURE 4. (Colour online) Streamwise distribution at $T = 2.5$ of the induced velocity v (a) and its streamwise derivative $\partial v/\partial X$ (b) at $Y = 3.4$, $Z = 0$; (c) wall-normal distribution of $\partial v/\partial X$ at $X = 2.8$, $Z = 0$.

3. Comparison with flow experiments

To demonstrate the universality of the mechanism the model results are compared with current flow visualization in a pipe and with previous visualization obtained in a channel.

3.1. *Pipe flow experiments*

The water pipe facility is detailed in Philip & Cohen (2010). The flow rate can be controlled to maintain a laminar flow for Re ($Re = U_{cl}R/\nu$) within the range of 250–3000 $\pm$ 1 %. Here U_{cl} and $R = 9.8$ mm are the centreline velocity and pipe radius and ν is the kinematic viscosity. Water-soluble dye (having water density) is injected perpendicularly to the pipe wall through a 0.8 mm diameter hole at a downstream distance of $114R$, where the flow is close to fully developed having a parabolic profile. The average injection velocity normalized by U_{cl} is v_0. The ratio between volume fluxes of disturbance to base flow is between 0.17 and 0.66 %. Two perpendicular views are simultaneously captured by a camera and an inclined mirror installed close to the pipe. The upstream end of the picture is two diameters downstream from the point of injection.

From flow visualization, the thickness (δ) of the CVP, the separation distance between the vortices ($2d_0$) and the streamwise wavelength (λ) are deduced to be 0.59, 1.1 and 5.9 mm, respectively. The shear of the base flow is taken as the average shear in the cross-section of the pipe ($\Omega \approx -U_{cl}/R = -25$ (s^{-1}), $Re = 2500$) and the magnitude of the initial streamwise vorticity is estimated as the ratio between the

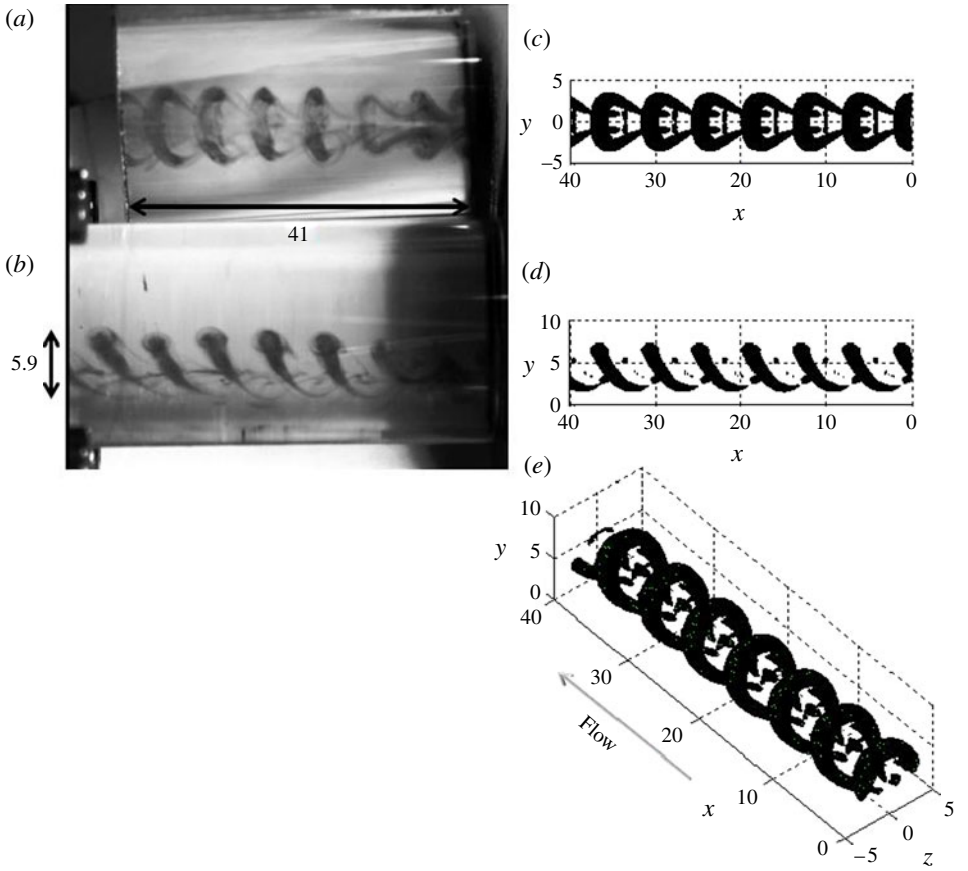

FIGURE 5. Comparison between the model and pipe flow experiments: (*a*,*b*) views of water pipe flow experiments following the evolution of a packet of hairpins from a laminar flow subjected to a cross-stream jet injection; (*c*,*d*) corresponding results with $Q/Q_{max} = 0.115$ and $T = 5.75$, following the temporal evolution of a packet of hairpins from a wavy spanwise vortex sheet imposed on a CVP embedded in simple shear. The flow parameters used in the simulation are obtained from the experiment: $Re = 2500$, $\Omega = -25$ (s^{-1}), $\varepsilon = 11.8$, $\delta = 0.59$ mm, $d_0 = 0.55$ mm, $\lambda = 5.9$ mm, $a_0 = 0.5$ and $h_0 = 0.5\delta$. (*e*) An isometric view of the packet. Dimensions in the figure are in millimetres. Flow from right to left.

injection velocity $v_0 = 0.7$ and the CVP thickness, i.e. $\varepsilon \approx (v_0 U_{cl}/\delta)/\Omega \approx v_0 R/\delta = 11.8$. It should be noted that the role of h_0 and a_0 is secondary: as their values are decreased/increased, the entire process is delayed/preceded.

Comparison between the pipe flow experiment and the model results is shown in figure 5. The packet of hairpins obtained experimentally is shown in figure 5(*a*,*b*). The corresponding model results are shown in figure 5(*c*,*d*), respectively. A very good agreement with respect to the characteristics of the packet is observed, indicating that the model is capable in capturing the main mechanisms involved in the packet evolution. An isometric view of the model-obtained packet is shown for completeness in figure 5(*e*). The encouraging agreement between our unbounded (having no walls) Cartesian model and the pipe flow results emphasizes its universality.

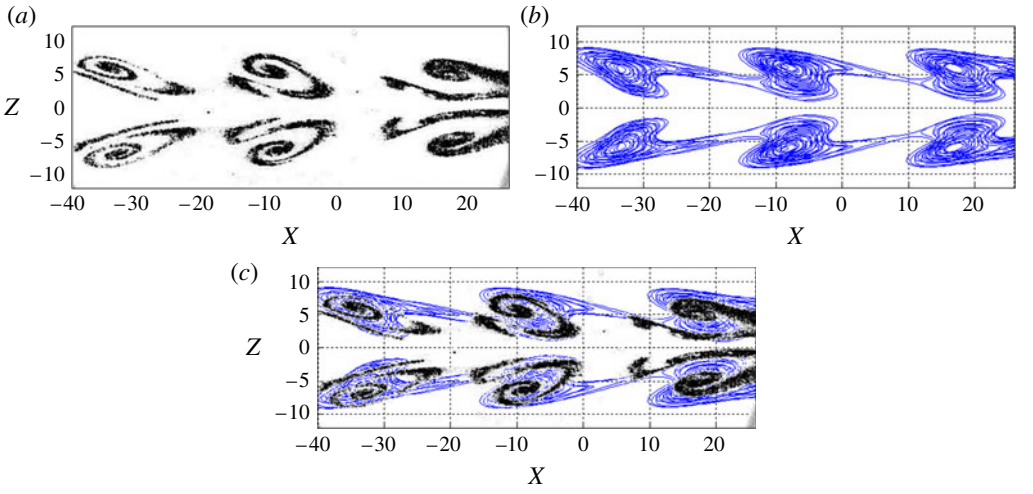

FIGURE 6. (Colour online) Comparison between the model and channel flow experiments. (*a*) Top-view visualization of a laminar air channel flow subjected to a cross-stream jet injection (reproduced from figure 2.12*b*, Philip 2009). (*b*) The corresponding model results illustrated by isocontours of Q at $T = 5$ and $Y = 1$ to $Y = 3$. The flow parameters are: $Re = 1660$, $\Omega = -40$ (s^{-1}), $\varepsilon = 7.5$, $\delta = 1$ mm, $d_0 = 10$ mm, $\lambda = 25$ mm, $a_0 = 1$ and $h_0 = 5$ mm. (*c*) The experimental visualization superimposed on the model results. All dimensions are normalized by δ. Flow from right to left.

3.2. *Channel flow experiments*

The air channel flow facility having a cross-section of 600 mm × 50 mm is detailed by Philip (2009). The Reynolds number is based on the centreline velocity (U_{cl}) and the half-channel height $h = 25$ mm. Disturbances were introduced into the laminar Poiseuille flow by continuous air injection through a streamwise slot (57 mm × 1 mm), drilled in the bottom wall. The disturbances were visualized by adding tracer particles to the secondary flow and illuminating them in the X–Z plane by a laser sheet. Flow visualization covers a distance of 1.5–4 h downstream of the injection location.

Similarly to the pipe flow experiments, the thickness (δ) of the CVP, the separation distance between the vortices ($2d_0$) and the streamwise wavelength (λ) are deduced from flow visualization to be 1, 10 and 25 mm, respectively, for the case in which $Re = 1660$ (corresponding to $U_{cl} = 1$ m s^{-1}) and the normalized injection velocity is $v_0 \approx 0.3$ (based on Philip (2009, figure 2.12*b*)). The shear of the base flow and the magnitude of the initial streamwise vorticity are estimated to be $\Omega \approx U_{cl}/h = -40$ s^{-1} and $\varepsilon \approx v_0 h/\delta = 7.5$, respectively.

Comparison between the channel flow experiments and the model results is shown in figure 6. The experimental top view visualization are taken from figure 2.12 in Philip (2009) and shown in figure 6(*a*). The corresponding model results are shown in figure 6(*b*) and are also superimposed on the experimental results in figure 6(*c*). A very good agreement is observed between the previously obtained channel flow experiments and the results of our unbounded Cartesian model, further supporting its universality.

4. Comparison with DNS transition in Couette flow

To further validate the universality of the proposed mechanism, we compare the results of the model with DNS results simulating transition in Couette flow, treated as

'experimental' results. We have used Gibson's well-tested 'Channelflow' DNS software (Gibson 2012). The simulation code is pseudospectral, using $N_x = 256$ and $N_z = 64$ Fourier modes in the x and z directions, respectively, and $N_y = 81$ Chebyshev modes in the y direction with no slip and impermeability on the walls at $y = \pm 1$ (length scales are normalized by the half-channel height, h). The streamwise and spanwise dimensions of the computational domain are 10π and 2π, respectively. Since the 3/2 rule is applied to remove aliasing, the number of corresponding Fourier modes is $N'_{x,z} = 2/3N_{x,z}$. The time step is chosen to obtain an initial Courant–Friedrichs–Lewy (CFL) number of 0.17.

It is well known that Couette and pipe flows are linearly stable. However, with a proper combination of linearly decaying modes, a significant transient growth can be achieved (through a linear mechanism, e.g. Butler & Farrell 1992; Schmid & Henningson 1994; Biau & Bottaro 2004; Ben-Dov & Cohen 2007; Eckhardt *et al.* 2007) and trigger nonlinear instabilities before ultimately decaying due to viscous effects. Nevertheless, linear mechanisms alone are not sufficient to trigger transition (e.g. Gustavsson 2009).

We have used an odd (antisymmetric with respect to the y-axis) initial disturbance (e.g. Brandt & de Lange 2008), which includes streamwise independent modes having a spanwise wavenumber of one. This combination of modes forms two pairs of CVPs (a total of four streamwise vortices). In this example the Reynolds number is $Re = U_w h/\nu = 1000$, where U_w is the velocity of the wall. The induced velocity of the CVPs destabilizes the base flow by creating a wall-normal inflection point at the centre ($y = 0$). To trigger instability, an infinitesimal 2D wavy disturbance having a streamwise wavenumber of one has been added. Figure 7 shows results obtained by the simulation. Only half of the domain is shown since the structures evolve symmetrically with respect to the y-axis. Time is normalized by h/U_w. At $T = 10$ (figure 7*a*) the CVP experiences a streamwise wavy modulation, which is enhanced by $T = 14$ (figure 7*b*). At $T = 24$ (figure 7*c*) streamwise-periodical spanwise vortical segments are formed above the wavy CVP which later join with the streamwise vortical elements situated beneath them. Consequently, a packet of hairpins is formed ($T = 35$, figure 7*d*). The packet further intensifies and the hairpin 'heads' become more localized having a shape of loops ($T = 45$, figure 7*e*). Shortly afterwards (not shown here) the flow becomes turbulent.

Striking similarities of the CVP temporal evolution between the model (figure 3) and the transition obtained by DNS (figure 7) are observed, despite the differences in the initial conditions and the absence of walls in the former. The physical process of the formation of a packet of hairpins during the transition scenario is explained by our model, further demonstrating its universality and robustness. Moreover, the synthetically evolved hairpins and modulated streamwise vortices are in agreement with similar structures observed during transition scenarios obtained via DNS from the minimal seed (e.g. Cherubini *et al.* 2011*b*) and with coherent structures found on the edge states (e.g. Duguet *et al.* 2012).

5. Conclusions

It has been shown that the three flow elements are sufficient to explain the physical mechanism of the formation of packets of hairpin vortices. Comparison between our simple Cartesian unbounded (having no walls) model, which contains the three flow elements, with experimental results for pipe and channel flows on the one hand and DNS of transition in Couette flow on the other hand suggests that the model is

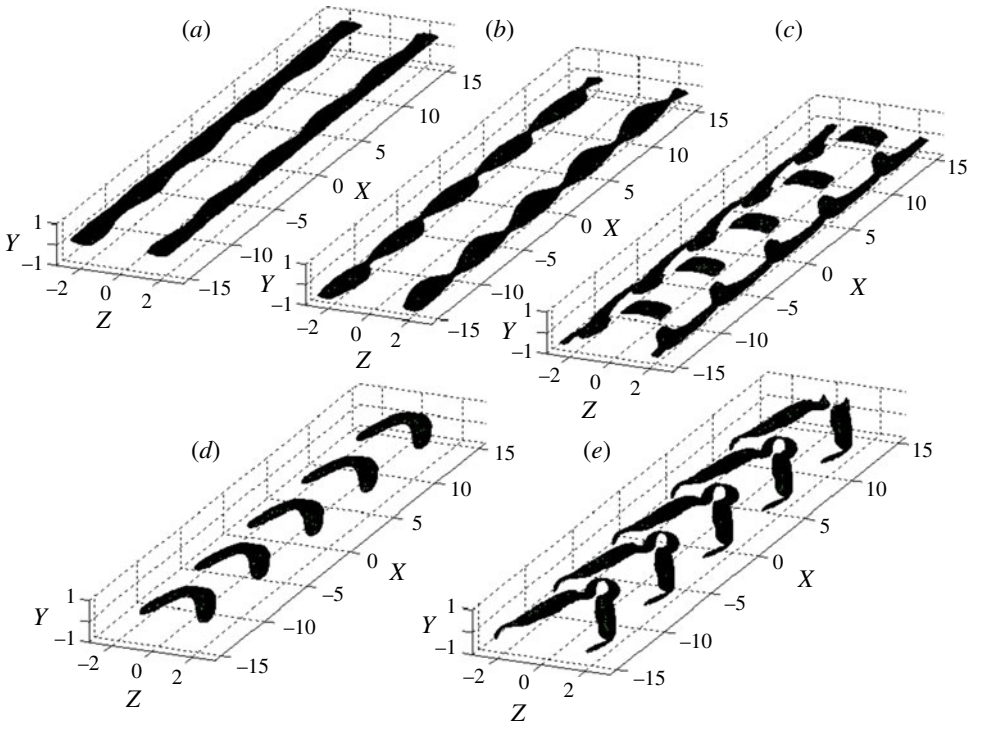

FIGURE 7. Temporal evolution of a packet of hairpins obtained by the 'Channelflow' DNS for Couette flow: (*a*) $T = 10$, $Q/Q_{max} = 0.6$; (*b*) $T = 14$, $Q/Q_{max} = 0.5$; (*c*) $T = 24$, $Q/Q_{max} = 0.3$; (*d*) $T = 35$, $Q/Q_{max} = 0.3$; (*e*) $T = 45$, $Q/Q_{max} = 0.11$. The structures are shown by isosurfaces of the Q definition. Only half of the domain is shown since the structures evolve symmetrically with respect to the y-axis (for each hairpin moving downstream in the top-half domain there is a hairpin moving in the opposite direction in the bottom-half domain).

universal and may explain the formation of packets of hairpins in various transitional shear flows and shed light on the formation of similar structures in fully developed turbulent shear flows.

Acknowledgements

The authors thank Ilia Shukhman for his contribution during the initial research stages and Jimmy Philip for his careful reading of the manuscript and valuable comments. This research was supported by the Israeli Science Foundation under Grant No. 1394/11.

REFERENCES

ACARLAR, M. S. & SMITH, C. R. 1987 A study of hairpin vortices in a laminar boundary layer. Part 1. Hairpin vortices generated by a hemisphere protuberance. *J. Fluid Mech.* **175**, 1–41.

ADRIAN, R. J., MEINHART, C. D. & TOMKINS, C. D. 2000 Vortex organization in the outer region of the turbulent boundary layer. *J. Fluid Mech.* **422**, 1–54.

ASAI, M., MINAGAWA, M. & NISHIOKA, M. 2002 The instability and breakdown of a near-wall low-speed streak. *J. Fluid Mech.* **455**, 289–314.

Ben-Dov, G. & Cohen, J. 2007 Instability of optimal non-axisymmetric base-flow deviations in pipe Poiseuille flow. *J. Fluid Mech.* **588**, 189–215.

Biau, D. & Bottaro, A. 2004 Transient growth and minimal defects: two possible initial paths of transition to turbulence in plane shear flows. *Phys. Fluids* **16**, 3515–3529.

Blackwelder, R. F. 1983 Analogies between transitional and turbulent boundary layers. *Phys. Fluids* **26**, 2807–2815.

Brandt, L. & de Lange, H. C. 2008 Streak interactions and breakdown in boundary layer flows. *Phys. Fluids* **20**, 024107.

Butler, K. M. & Farrell, B. F. 1992 Three-dimensional optimal perturbations in viscous shear flow. *Phys. Fluids* A **4**, 1637–1650.

Cherubini, S., De Palma, P., Robinet, J. -C. & Bottaro, A. 2010*a* Rapid path to transition via nonlinear localized optimal perturbations in a boundary-layer flow. *Phys. Rev.* E **82**, 066302.

Cherubini, S., De Palma, P., Robinet, J. -C. & Bottaro, A. 2011*a* Edge states in a boundary layer. *Phys. Fluids* **23**, 051705.

Cherubini, S., De Palma, P., Robinet, J. -C. & Bottaro, A. 2011*b* The minimal seed of turbulent transition in the boundary layer. *J. Fluid Mech.* **689**, 221–253.

Cherubini, S., Robinet, J. -C., Bottaro, A. & De Palma, P. 2010*b* Optimal wave packets in a boundary layer and initial phases of a turbulent spot. *J. Fluid Mech.* **656**, 231–259.

Chu, J. C. & Goldstein, D. B. 2012 Investigation of turbulent wedge spreading mechanism with comparison to turbulent spots. *AIAA Paper 2012-0751, Proceedings of the 50th AIAA ASM, Nashville, TN*, pp. 1–15. DOI: 10.2514/6.2012-751.

Cohen, J., Karp, M. & Shukhman, I. 2009 The formation of packets of hairpins in shear flows. *Proceedings of Global Flow Instability and Control IV, Crete, Greece* www.cfm.upm.es/resources/Crete-IV—Summary.pdf.

Cohen, J., Shukhman, I. G., Karp, M. & Philip, J. 2010 An analytical-based method for studying the nonlinear evolution of localized vortices in planar homogenous shear flows. *J. Comput. Phys.* **229**, 7765–7773.

Duguet, Y., Schlatter, P., Henningson, D. S. & Eckhardt, B. 2012 Self-sustained localized structures in a boundary-layer flow. *Phys. Rev. Lett.* **108**, 044501.

Eckhardt, B., Schneider, T. M., Hof, B. & Westerweel, J. 2007 Turbulence transition in pipe flow. *Annu. Rev. Fluid Mech.* **39**, 447–468.

Gibson, J. F. 2012 Channelflow: a spectral Navier–Stokes simulator in C++. *Tech. Rep.* University of New Hampshire, Channelflow.org.

Gustavsson, L. H. 2009 Nonlinear wave interactions from transient growth in plane-parallel shear flows. *Eur. J. Mech. (*B*/Fluids)* **28**, 420–429.

Haidari, A. H. & Smith, C. R. 1994 The generation and regeneration of single hairpin vortices. *J. Fluid Mech.* **277**, 135–162.

Head, M. R. & Bandyopadhyay, P. 1981 New aspects of turbulent boundary-layer structure. *J. Fluid Mech.* **107**, 297–338.

Hof, B., de Lozar, A., Avila, M., Tu, X. & Schneider, T. M. 2010 Eliminating turbulence in spatially intermittent flows. *Science* **327**, 1491–1494.

Hunt, J. C. R., Wray, A. A. & Moin, P. 1988 Eddies, stream, and convergence zones in turbulent flows. *Center for Turbulence Research, Report CTR-S88*, pp. 193–208.

Hutchins, N., Hambleton, W. T. & Marusic, I. 2005 Inclined cross-stream stereo particle image velocimetry measurements in turbulent boundary layers. *J. Fluid Mech.* **541**, 21–54.

Levinski, V. & Cohen, J. 1995 The evolution of a localized vortex disturbance in external shear flows. Part 1. Theoretical considerations and preliminary experimental results. *J. Fluid Mech.* **289**, 159–182.

Malkiel, E., Levinski, V. & Cohen, J. 1999 The evolution of a localized vortex disturbance in external shear flows. Part 2. Comparison with experiments in rotating shear flows. *J. Fluid Mech.* **379**, 351–380.

Marusic, I. 2001 On the role of large-scale structures in wall turbulence. *Phys. Fluids* **13**, 735–743.

Marusic, I., Mathis, R. & Hutchins, N. 2010 Predictive model for wall-bounded turbulent flow. *Science* **329**, 193–196.

PEIXINHO, J. & MULLIN, T. 2007 Finite-amplitude thresholds for transition in pipe flow. *J. Fluid Mech.* **582**, 169–178.

PHILIP, J. 2009 The relationship between streaks and hairpin vortices in subcritical wall bounded shear flows. PhD thesis, Technion - Israel Institute of Technology.

PHILIP, J. & COHEN, J. 2010 Formation and decay of coherent structures in pipe flow. *J. Fluid Mech.* **655**, 258–279.

PHILIP, J., SVIZHER, A. & COHEN, J. 2007 Scaling law for a subcritical transition in plane poiseuille flow. *Phys. Rev. Lett.* **98**, 154502.

RAYLEIGH, L. 1880 On the stability, or instability, of certain fluid motions. *Proc. Lond. Math. Soc.* **1**, 57–72.

RIST, U. 2012 Visualization and tracking of vortices and shear layers in the late stages of boundary-layer laminar-turbulent transition. *AIAA paper 2012-0084, Proceedings of the 50th AIAA ASM, Nashville, TN*, pp. 1–20. DOI: 10.2514/6.2012-84.

ROBINSON, S. K. 1991 Coherent motions in the turbulent boundary layer. *Annu. Rev. Fluid Mech.* **23**, 601–639.

SCHMID, P. J. & HENNINGSON, D. S. 1994 Optimal energy density growth in Hagen–Poiseuille flow. *J. Fluid Mech.* **277**, 197–226.

SKOTE, M., HARITONIDIS, J. H. & HENNINGSON, D. S. 2002 Varicose instabilities in turbulent boundary layers. *Phys. Fluids* **14**, 2309–2323.

STRAND, J. S. & GOLDSTEIN, D. B. 2011 Direct numerical simulations of riblets to constrain the growth of turbulent spots. *J. Fluid Mech.* **668**, 267–292.

SUPONITSKY, V., COHEN, J. & BAR-YOSEPH, P. Z. 2005 The generation of streaks and hairpin vortices from a localized vortex disturbance embedded in unbounded uniform shear flow. *J. Fluid Mech.* **535**, 65–100.

SWEARINGEN, J. D. & BLACKWELDER, R. F. 1987 The growth and breakdown of streamwise vortices in the presence of a wall. *J. Fluid Mech.* **182**, 255–290.

THEODORSEN, T. 1952 Mechanism of turbulence. In *Proceedings of Second Midwestern Conf. on Fluid Mech.* pp. 1–19.

WU, X. & MOIN, P. 2009 Direct numerical simulation of turbulence in a nominally zero-pressure-gradient flat-plate boundary layer. *J. Fluid Mech.* **630**, 5–41.

ZHOU, J., ADRIAN, R. J. & BALACHANDAR, S. 1996 Autogeneration of near-wall vortical structures in channel flow. *Phys. Fluids* **8**, 288–291.

ZHOU, J., ADRIAN, R. J., BALACHANDAR, S. & KENDALL, T. M. 1999 Mechanisms for generating coherent packets of hairpin vortices in channel flow. *J. Fluid Mech.* **387**, 353–396.